# Superhydrophobic surface coating on electrospun polypropylene membrane to treat high salinity water in membrane distillation

Jing Yi Chin, Guang Hui Teoh, Abdul Latif Ahmad and Siew Chun Low

## ABSTRACT

Membrane distillation (MD) is an advantageous separation process compared with pressure-driven technologies and was subsequently introduced to treat aquaculture wastewater. Harnessing a superhydrophobic membrane in an MD process is of extreme importance to prevent membrane wetting. In this work, the electrospun polypropylene (PP) membrane was surface modified by depositing an additional coating of PP via the solvent-exchange method, thereby improving the membrane's superhydrophobicity. Layer-by-layer deposition of PP caused the formation of uniform polymer spherulites on the membrane surface, which levelled up the membrane's surface roughness. A superhydrophobic surface was achieved by applying a single-layered PP coating, with static water contact angle of 152.2° and sliding angle of 12.5°. While all membranes achieved almost perfect salt rejection (up to 99.99%), the MD permeate flux improved by 30%, average of 13.0 kg/m$^2$ h, when the single-layered PP-coated membrane was used to treat the high salinity water in both 2 and 60 hr MD processes. Further layers of coating resulted in larger size of PP spherulites with higher sliding angle, followed by lowered flux in MD. The evenness of the surface coating and the size of the aggregate PP spherulites (nano-scaled) are two predominant factors contributing to the superhydrophobicity character of a membrane.

**Key words** | anti-wetting membrane, homogeneous roughness, sliding contact angle, solvent-exchange coating, superhydrophobic

**Jing Yi Chin**
**Guang Hui Teoh**
**Abdul Latif Ahmad**
**Siew Chun Low** (corresponding author)
School of Chemical Engineering, Engineering Campus,
Universiti Sains Malaysia,
Seri Ampangan, 14300 Nibong Tebal, Pulau Pinang, Malaysia
E-mail: *chsclow@usm.my*

## HIGHLIGHTS

- PP was surface-coated on the electrospun membrane via solvent-exchange.
- Layer-by-layer PP deposition formed tiny and uniform spherulites on membrane surfaces.
- Nano-scaled and an even surface roughness rendered modified membranes superhydrophobic.
- Membrane distillation flux improved by 30% in treating high salinity water.

doi: 10.2166/wst.2020.528

## GRAPHICAL ABSTRACT

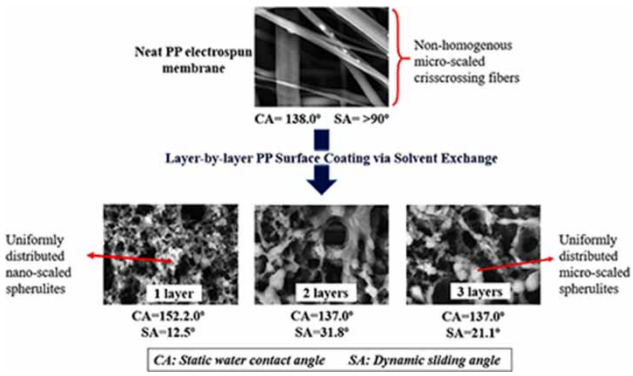


## INTRODUCTION

Aquaculture has emerged to be the most intensively growing sector to provide food for populations around the world, as global capture fishery production has reached a ceiling. The upward development of this aquatic species cultivation industry has a downside, associated with concerns about effectively treating its wastewater (Liu *et al.* 2019). Membrane distillation (MD) was brought to light as a promising aquaculture wastewater treatment technology, by virtue of its ability to treat high salinity water (Li *et al.* 2017) and nitrogenous waste (Qu *et al.* 2013; Boubakri *et al.* 2015). MD is also easily scalable and able to function with low grade heat sources. Different from pressure-driven wastewater treatment technology such as reverse osmosis, the MD process is thermally driven, which extensively reduces the fouling concern. Also, permeate quality of MD will not be affected by salinity of its feed (Koschikowski *et al.* 2003). To maintain functionality of MD, the membrane used in MD has to be anti-wetted, highly porous and of low thermal conductivity. Also, it must be able to withstand cross-membrane temperature difference.

With that in mind, polypropylene (PP), a hydrophobic polymer with thermal conductivity of 0.17 W/(m K) (the lowest among other common polymeric materials) (Wang & Chung 2015) appears to be a suitable candidate to fabricate the membrane. In addition, the manufacturing cost of PP is lower, and its thermoplastic properties would render the membrane to stay intact over the thermal separation process. A study by Shao *et al.* (2019) confirmed this claim when they performed MD using a superhydrophobic modified PP membrane. The membrane performed excellently in blocking water penetration and exhibited stable permeating flux under low feed rate and concentrated salt solution. A highly porous membrane, on the other hand, can be fabricated via electrospun method. An electrospun membrane is beneficial over a membrane produced through traditional phase inversion for usage in MD application as its thickness can be customized. Also, it has higher porosity for better vapor permeability contributed by its interconnected open pore structure. The overlapping fibers of an electrospun membrane also create a rough surface which is favorable to increase hydrophobicity. Nonetheless, the electrospun membrane faced a critical challenge in which water would adhere strongly on its surface regardless of its high static water contact angle, known as the 'petal effect'. This phenomenon was observed in a study of Liao *et al.* (2013), whereby the water droplet retained a spherical shape and did not roll off even when the electrospun membrane was tilted upside down. The petal effect will intensify the wetting issue and temperature polarization. As severity of temperature polarization increased, temperature gradient which accounts for the separation driving force across the membrane would decrease, resulting in declining permeate flux.

To resolve the issue of water adhesion on the membrane surface, several techniques have been implemented to further enhance the membrane's hydrophobicity by tuning surface morphologies of the membrane, including plasma treatment (Yang *et al.* 2014), imprinted patterned membrane surface (Teoh *et al.* 2020) and many more. On top of this, layer-by-layer assembly (LbL) stands out as a laudable modification technique to furnish the membrane with superhydrophobic characteristics. Other than handy control over a multi-layer thin film at nanometer scale, LbL offers

myriad choices of usable materials and technical applicability (Ariga *et al.* 2019). For instance, by attaching 1H,1H,2H,2H-perfluorodecyltriethoxysilane on $SiO_2$ nanoparticles loaded PP membrane, water contact angle (WCA) of the membrane escalated from 118° to 159°, as reported by Wang *et al.* (2019). Similarly, as produced by Seyed Shahabadi *et al.* (2017) dual layer membranes with electrospun polyvinylidene fluoride-co-hexafluoropopylene nanofibers as support layer followed by electrospraying hydrophobic functionalized $TiO_2$ nanoparticles on the surface of the support layer were able to attain WCA greater than 155°. Also, an electrospun polyvinylidene fluoride (PVDF) was endowed with superhydrophobic properties after deposition of a porous thin amorphous PP film on the surface via vacuum filtration (Deng *et al.* 2019). These modification methods, however, require incorporation of extrinsic hydrophobic materials which are prone to abrasion after long operation duration. In lieu of that, a simple LbL technique in the form of solvent-exchange with usage of minimal materials was developed and proven to successfully improve surface roughness and homogeneity of membranes. For example, Franco *et al.* (2008) spin-coated a thin layer of PP coating onto the PP membrane via solvent-exchange method, which successfully brought up contact angle (CA) of the membrane to 169°. Similarly, a surface coated with low density polyethylene (LDPE), utilizing cyclohexanone as non-solvent, has also resulted in an astonishing static WCA of 173° (Lu *et al.* 2004). Via this chemical treatment, the LDPE formed a floral-like crystal structure, which contributed to the membrane's superhydrophobicity (Lu *et al.* 2004).

Gathering all the information, the main research gap is that studies regarding MD desalination applications using PP membrane are extremely scarce. Moreover, none of the research employing the facile solvent-exchange technique to enhance membrane superhydrophobicity was applied on MD separation. In addition, electrospun membranes harnessed for MD in most of the research works are usually made of PVDF. Hence, this study focused on modifying a commercial PP electrospun membrane via the simple and inexpensive solvent-exchange coating method to be used to desalt high salinity water in MD. This work aimed to resolve the water pinning effect on the electrospun PP membrane and render it superhydrophobic while maintaining high membrane porosity which is favorable for MD operations. In consideration of polymer compatibility, PP polymer was used as the coating dope. The electrospun PP membranes were layer-by-layer coated with one, two or three layers of PP polymer. Subsequently, their anti-wetting resistance in direct contact membrane distillation (DCMD) separation was evaluated, with salt concentration of feed solution mimicking that of aquaculture seawater (35 g/L). Also, membranes' surface and cross-sectional morphologies were also analyzed to assess the qualitative changes of the surface modified membranes.

## METHODS

### Materials

A commercial PP electrospun membrane (pore size: 10 μ, 200 × 200 mm) was supplied by Sterlitech (USA), while granulated PP polymer (Titanpro 6331) provided by Lotte Chemical Titan (Malaysia) has been used for membrane surface coating. Xylene (ACS reagent, ≥98.5% xylenes + ethylbenzene) from Sigma-Aldrich (USA) and methyl ethyl ketone (MEK) from Merck (USA) acted as solvent and non-solvent respectively.

### Membrane surface modification via solvent-exchange coating

A preliminary study was carried out using 10, 20, 25 and 35 mg/mL PP as coating dope and morphologies of respective coated membranes were observed under scanning electron microscopy. Based on the observation, 20 mg/mL PP is known as the optimum concentration for solvent-exchange coating. A concentration below the optimum level produced discrete patches of coating layer while concentration above optimum level led to overly crowded PP spherulite lumps. To prepare 20 mg/mL PP solution, 0.5 g of granulated PP was dissolved in 25 mL of xylene, heated at 120 °C with constant stirring at 350 rpm under a silicon oil bath. Prior to coating, the commercial neat PP membrane was clamped horizontally on a stainless steel holder in order to perform one-side surface coating of the membrane by using an automated dip coater. MEK and PP solution were poured separately and evenly into two respective stainless steel containers, with the container containing PP solution placed on a heat plate with temperature set at 90 °C. This is to ensure the consistency of coating temperature for every single coating performed. Immediately after the solvent and non-solvent were poured into their respective containers, the neat membrane was first immersed in MEK for 30 s, followed by contacting one side of the membrane surface with PP solution for 10 s. Within this contact duration, biaxial shaking of the container containing PP coating dope was performed to ensure even deposition of

PP on the membrane surface. Subsequently, the coated membrane was transferred to a vacuum oven at 70 °C and approximately 0.33 Pa to control the solidification rate of PP and to avoid the heterogeneous oxidation of PP. The membrane was left in the oven for 1 hr until the coated PP layer turned white, indicating full solidification. For membranes coated with two and three layers, the coating was performed layer-by-layer. The double and triple layered membranes were prepared by repeating the above steps once and twice, respectively. To ensure reproducibility of the solvent-exchange surface modification, each modified membrane was reproduced several times by repeating coating steps exactly as mentioned above. Characterizations were repeated on the membranes and their averaged results are reported.

Surface and cross-sectional morphologies of the membranes, before and after PP coating, were analyzed using scanning electron microscopy (SEM, TM3000, Hitachi, Japan). Owing to the thermoplastic characteristic of PP, membrane samples for cross-section observation have to be cracked with the following sequence: immerse samples in ethanol, followed by distilled water, then liquid nitrogen. Wettability of the membrane was evaluated using results from surface static CA and sliding angle (SA). CA and SA of the membrane were measured by using the sessile drop method with a surface meter (Lauda Surface Analyzer 200, Germany). Ten microliters of distilled water was dropped at various points on the sample surfaces, at which points the CA and SA results were taken and are reported as average values. As for surface roughness, a determining factor that will affect CA and SA of the membrane, samples were evaluated using atomic force microscopy (AFM, Bruker, Dimension Edge, Tap 300-G, Germany). The membrane's surface roughness was measured using a non-contact head with scanning area of 20 μm × 20 μm. From the AFM data, the homogeneity of the membrane surfaces could also be observed. For porosity measurement, membrane samples were soaked in 2-butanol for 2 hr. Weight of wetted membrane was taken prior to drying it completely in an oven. The overall porosity of membranes was calculated using Equation (1):

$$\varepsilon = \frac{m_n/\rho_n}{(m_n/\rho_n) + (m_p/\rho_p)} \times 100\% \quad (1)$$

where $\varepsilon$ indicates the overall porosity, $m_n$ is the mass of 2-butanol absorbed by the membrane, $\rho_n$ is the density of 2-butanol (0.81 g/cm$^3$), $m_p$ is the mass of dry membrane, and $\rho_p$ is the density of PP (0.90 g/cm$^3$).

### Direct contact membrane distillation performance test

Mimicking the salinity of aquaculture seawater, salt solution with concentration of 35 g/L was prepared as feed solution while deionized water was circulated as permeate in 2 hr (short term) and 60 hr (long term) DCMD separation tests. During the tests, the coated side of membranes were installed to face the hot feed in the module. The feed solution was kept at 60 °C while the permeate stream was maintained at 20 °C. Running at a flow rate of 0.3 L/min for both hot feed and cold permeate streams, the separation flux ($J$, kg/m$^2$ h) was calculated by dividing mass of water transported from feed to permeate ($\Delta m$, kg) by time interval ($\Delta t$, h) and effective membrane area ($A = 0.00089$ m$^2$), as denoted in Equation (2).

$$J = \frac{\Delta m}{A\Delta t} \quad (2)$$

Conductivity of permeate, an indicator of the membrane's ability to restrain penetration of salt from feed to permeate, was measured by a conductivity meter (Eutech Cond 6 +, Thermo Scientific) every 15 min throughout the DCMD process. Salt rejection ($R$), was then evaluated using the formula defined in Equation (3).

$$R = \left(1 - \frac{C_p}{C_f}\right) \times 100\% \quad (3)$$

where $C_p$ denotes conductivity of permeate while $C_f$ represents conductivity of the feed.

## RESULTS AND DISCUSSION

In this work, the surface modified electrospun membranes are denoted as neat PP, PP/6331-L1, PP/6331-L2 and PP/6331-L3 respectively. PP represents the polypropylene electrospun membrane, 6331 refers to the PP polymer coated on the membrane surface, and 'L' indicates 'layer' followed by number of coating layers. Scrutinizing membrane morphologies under SEM, the neat PP membrane (Figure 1(a)-left) presented a surface of intersecting PP fibers in micrometer diameters. The irregularity of fiber sizes and crisscrossing rendered the membrane surface a micro-scaled, inhomogeneous roughness. An electrospun membrane, as seen in the cross-section SEM images

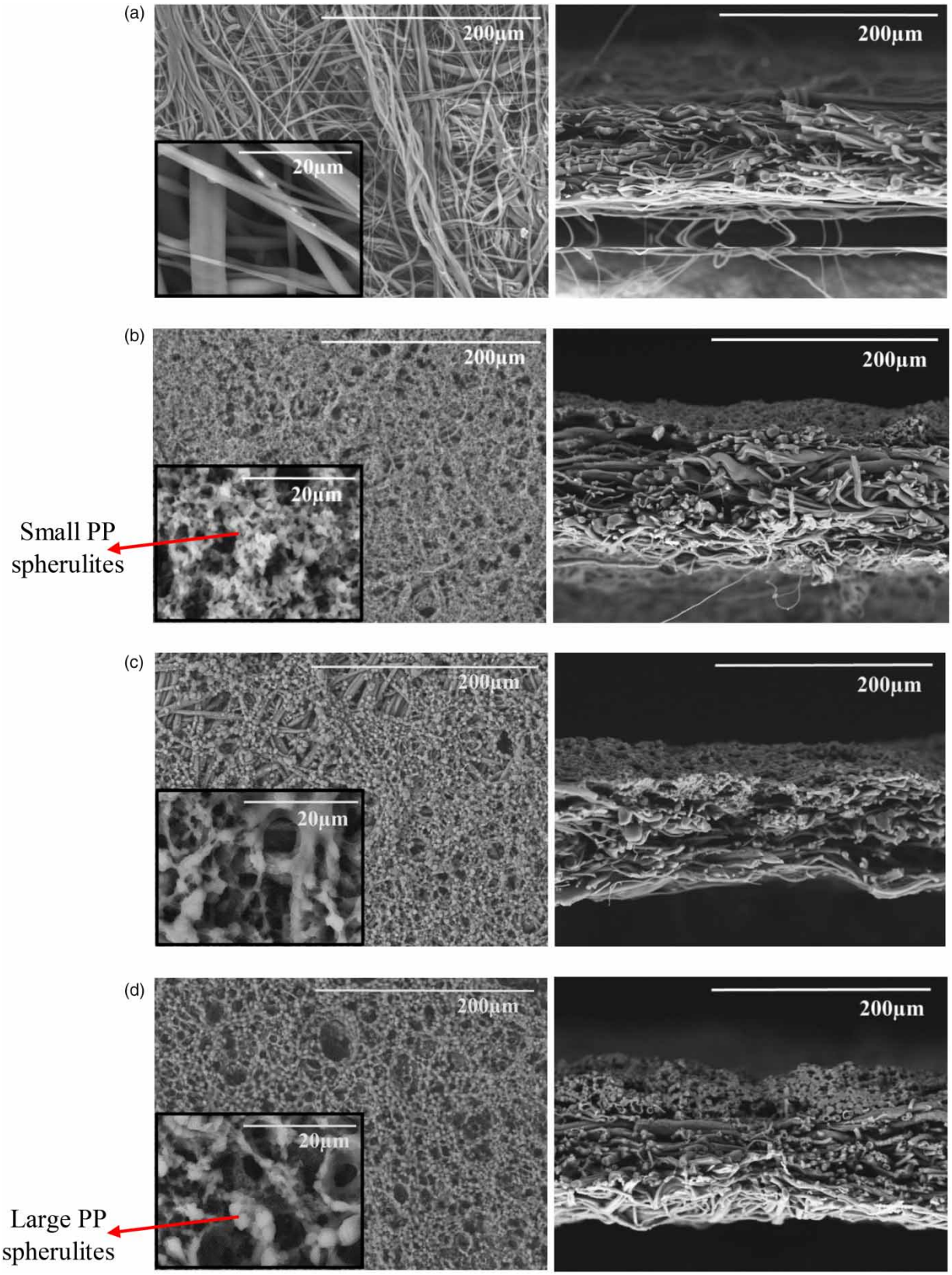


**Figure 1** | SEM micrograph of surface (left images) and cross-sectional (right images) of (a) neat PP, (b) PP/6331-L1, (c) PP/6331-L2 and (d) PP/6331-L3 membranes.

(Figure 1(a)-right), has no regular longitudinal pores running through the inner section.

After PP polymer was surface-coated on the membrane surface, the virgin membrane surface morphology can no longer be seen in Figure 1(b)–1(d) (left images), implying a full coverage of PP polymer on the membrane surfaces. Different from neat PP membrane, the coated membranes demonstrated agglomeration of polymer clusters pervading the surface. These agglomerates are termed as spherulites, indicating aggregates of primary crystallites of spherical shape (van der Meer 2003). The agglomeration was formed through PP crystallization with the aid of non-solvent MEK, which induces polymer phase separation into polymer-rich and polymer-lean phases. When heated, the PP polymer chains can move easily, thereby crystal nuclei formed in the polymer-rich phase. The solvent then evaporated from the polymer-lean phase, leading to the transformation of crystal nuclei into spherulites. Since MEK is more volatile than the solvent xylene, its presence increased the solvent evaporation rate. Consequently, it decreased the time required for crystal formation, thus forming smaller spherulites (Erbil *et al.* 2003), as seen from the inserted image in Figure 1(b) (left). This smaller size of spherulites contributed to nano-scaled roughness on the membrane surface.

On the other hand, the ability of PP polymer to be firmly layered on the membrane surface relies on the disentangle and re-entanglement of PP polymer chain. During surface coating, part of the membrane has actually melted when in contact with the high temperature PP solution containing xylene. At this point, polymer chains on the membrane surface and coating dope have partially disentangled (Krajenta *et al.* 2016) and coexist in the solution. As the solution cooled down, entanglements in PP recovered via reptation motions of PP chains (Krajenta *et al.* 2019). The re-entanglement of PP chains is a non-discriminative process, whereby the PP polymers did not only entangle among their original molecular chains, but also with chains of their counterparts, meaning at the stage of re-entanglement, PP chains on the membrane surface entangled with chains of coating PP polymer, hence grabbing the PP coated layer firmly on the membrane surface. At the same time, the coating polymer chains entangled among themselves, resulting in a continuous network of spherulites holding together by a stick- and branch-like structure layering the membrane surface. Similarly, when stacking up the coating layers (Figure 1(c) and 1(d)), the mechanism by which the PP polymer chain partially disentangled and then re-entangled was replicated. As PP coating thickened, density of PP polymer chain entanglement was intensified. Owing to this phenomenon, there were fewer nucleation sites formed during multi-layer coating (Wang *et al.* 2009), leading to generation of larger spherulites (Figure 1(d)-left) as compared to the single-layer PP coating (Figure 1(b)-left) (Sawyer *et al.* 2008).

Indeed, mass transfer during MD process is highly dependent on the available voids in between the intersecting fibers. As voids present in membranes are vital to lower loss of conductive heat and to reduce mass transfer resistance of vapor across membranes in MD application, there was concern that the PP coatings would partially block the voids. Thus far, cross-sectional SEM of the surface-coated membranes (Figure 1(b)–1(d), right) depicted the coating layers stayed put on the membrane surfaces and showed no significant sign of penetration, indicating the porousness of membranes was not affected. In fact, neat PP membrane has porosity of $74.5 \pm 1.0\%$, whereas porosities for single, double and triple layers coated membranes were $75.7 \pm 2.8\%$, $74.8 \pm 1.4\%$ and $73.0 \pm 4.5\%$ respectively. These results supported the above discussion that the surface coatings will not jeopardize the porosity of the membrane, where influences of mass transfer resistance due to the proposed surface modification would be minimal.

Attributed to low surface energy of PP and surface roughness induced by the crisscrossing fibrous structure, neat PP membrane achieved CA of $138.0 \pm 3.6^\circ$, disclosing the membrane's hydrophobic character. Putting aside the ability of PP to repel water due to its hydrophobic nature, the CA and mobility of water on the membrane surface are highly governed by a three-phase contact line (TCL) existing between solid, liquid and air interfaces. As seen in Figure 1(a) (left SEM image), neat PP membrane comprises micro-scaled fibers. Though having high CA at 138.0°, the membrane has yet to achieve superhydrophobic state, indicating vastly present micro-scale re-entrants on its surface are too broad to entrap air effectively to lift up the solid–liquid interface. A relatively large portion of the water droplet still comes into contact with the electrospun fibers. Consequently, SA of neat PP membrane was strikingly high, with a record of >90° (Table 1), a feature that contradicts the superhydrophobic characteristic. In fact, the water droplet was pinned on the membrane surface even when the sample was turned upside down (180°). This is probably due to extreme inhomogeneity of roughness on the membrane surface, as the surface was configured by randomly arrayed intersecting fibers (Figure 1(a)-left). The non-homogeneity means that TCL on the membrane surface conforms to neither the Wenzel nor Cassie-Baxter wetting behavior model, but the co-existence of both. This is because despite

**Table 1** | Contact and sliding angles of neat and PP-coated membranes

| Samples | Contact angle (°) | | Sliding angle (°) | |
|---|---|---|---|---|
| Neat PP | 138.0 ± 3.6 |  | >90 |  |
| PP/6331-L1 | 152.2 ± 2.5 | 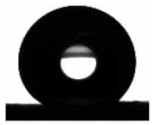 | 12.5 ± 5.3 |  |
| PP/6331-L2 | 147.8 ± 0.6 |  | 31.8 ± 11.7 |  |
| PP/6331-L3 | 137.0 ± 4.0 |  | 21.2 ± 7.0 |  |

theoretical conflict between Wenzel and Cassie-Baxter models, both models are analogously applicable merely to homogeneously rough surfaces. To investigate wetting behavior of a non-homogeneously rough surface, a sophisticated intermediate of Wenzel and Cassie-Baxter models, i.e. the Cassie-impregnating regime (Feng *et al.* 2008), should be embraced. A surface following the Cassie-impregnating regime (refers to neat PP membrane in present work) is considered to have the 'petal effect', and would be termed as a parahydrophobic surface. This type of membrane surface is noticed to have prominent characteristics of high CA, but at the same time, strong adhesion towards water (Table 1).

A usual characteristic of a parahydrophobic surface is that it has both uneven micro- and nano-scaled hierarchical topography. As proven by the AFM analysis, the surface morphology of neat PP membrane (Figure 2(a)) resembled this dual-scale topography, with surface roughness ($R_a$) of 0.428 μm. While micro-scaled peaks and valleys dominate, the existence of the intermittent nano-scaled roughness on the surface of neat PP membrane could not be neglected. In the area between the large micron distance peaks, the TCL interface produced on the membrane conforms to the Wenzel model, allowing water to penetrate into the asperities. At the same time, there is entrapped air between nano protrusions bolstering the solid–liquid interface, and thus, in contrast, reduced surface contact between the water and neat PP membrane. Nonetheless, the air pockets are isolated and not homogeneously distributed across the membrane surface, which leads to the continuity of TCL overall and contributes towards strong water adhesion (Lai *et al.* 2009).

The phenomenon in which water adheres firmly on the membrane surface is greatly undesired in MD application as it will aggravate severity of the wetting and temperature polarization issue. Creating an anti-wetting surface with 'lotus effect' hence became a primary mission in this work. By coating single or several layers of PP polymer onto the membrane surface, the modified electrospun membranes showed drastic abatement of water adhesion on their respective surfaces (Table 1). All surface-coated membranes had enhanced SA of below ~30°. The most straightforward implication of this improvement is that the PP coatings have successfully resolved the pilling problem of neat PP membrane, as depicted in Figure 3(b). As shown in Figure 3(a), the neat PP membrane displayed pilling fibers on its surface and these fibers were expected to lock water movement, so as to influence the SA performance of the membrane. These fibrous pillings on the hydrophobic electrospun PP membrane showed high biomimetic resemblance to *Cotula fallax* plant which has dense hydrophobic sericeous fibers with an approximate diameter of 5 μm covering the surfaces of leaves. The overlapping and intertwining of the plant's hairs created a mat-like structure that grabbed the water firmly even when water droplets expanded in volume during fog collection (Andrews *et al.*

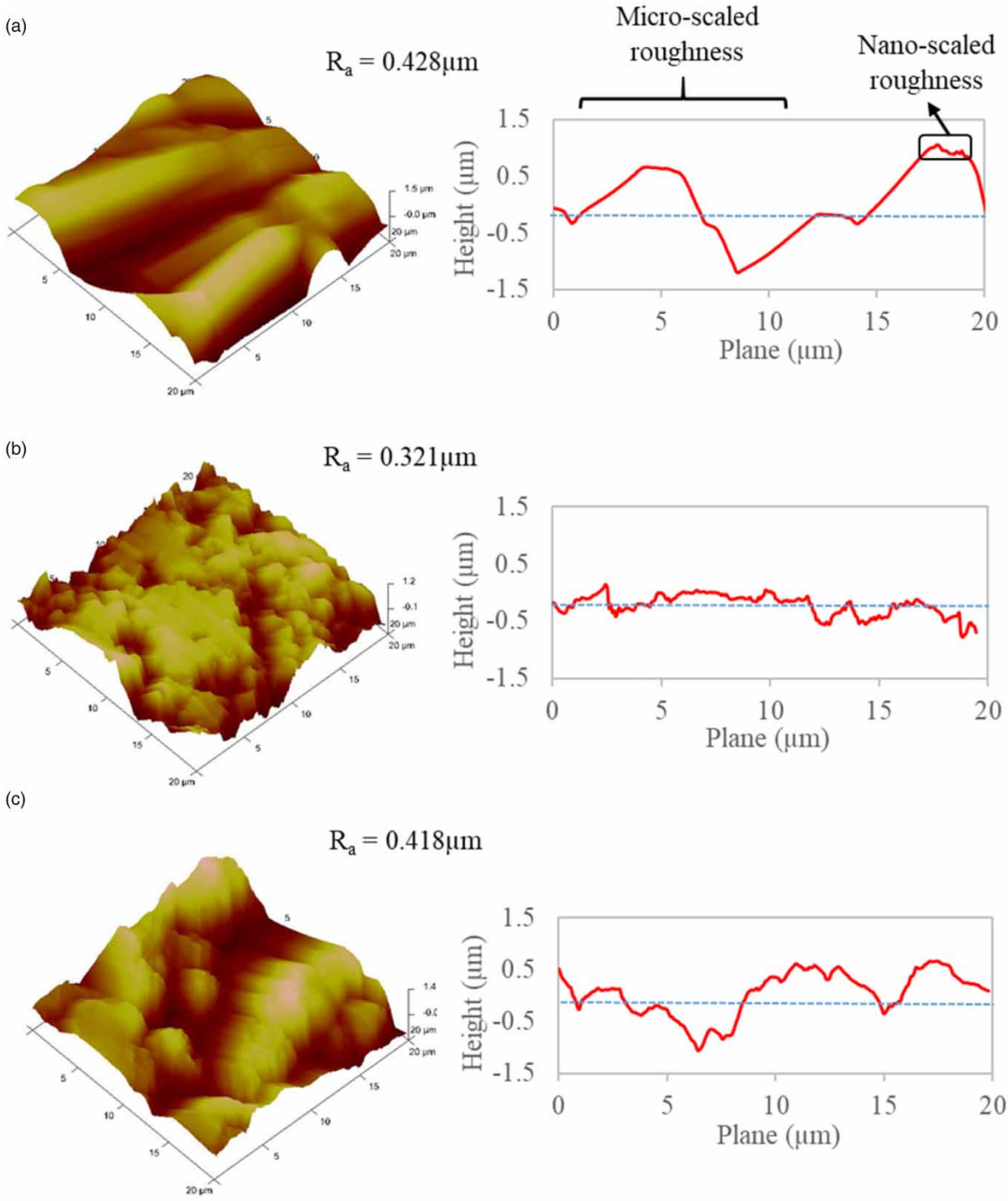


**Figure 2** | AFM analyses of (a) neat PP, (b) PP/6331-L1 and (c) PP/6331-L3 membranes.

2011). Similar to the *Cotula fallax* plant, hair-like fibers on the surface of neat PP membrane captured water droplets effectively, while adhesion force occurring along the groove of individual fibers underpinned the water even more strongly. During the experiment, an interesting scene was observed whereby a significant amount of water was added gradually to the water droplet originally pinned on the surface of neat PP membrane, tilted at position of 90°.

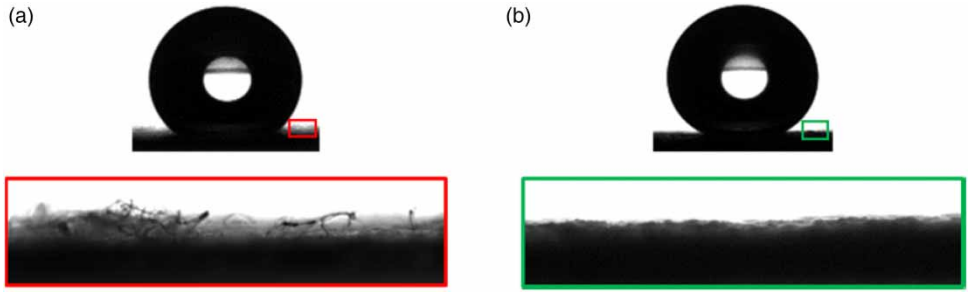


**Figure 3** | Close-up images of (a) neat membrane, (b) coated membrane.

The water droplet, however, showed no sign of sliding, even when expanded up to several magnitudes of its original volume.

While the multi-layered PP coating pronouncedly promoted water mobility on the membrane surfaces, the most notable improvement was achieved by the membrane with single PP coating layer (PP/6331-L1). As tabulated in Table 1, PP/6331-L1 successfully reached the superhydrophobic state, with recorded CA of $152.2 \pm 2.5^{\circ}$ and SA of $12.5 \pm 5.3^{\circ}$. This dramatic enhancement was attributed to the formation of homogeneous nano-scaled PP bumps on the membrane surface (Figure 1(b)). The homogeneity of roughness distributed on PP/6331-L1 was evidenced by AFM analysis (Figure 2(b)), in which the surface section showed a quasi-horizontal line decorated with evenly distributed nano-scaled valleys. As the distance between protuberances is greatly minimized (from micro- to nano-scaled), air can be trapped easily within, forming a large and continuous domain. The uniformly distributed air pockets then hinder impregnation of water into the nano valleys, thus effectively breaking up the contact in between solid and liquid phases, rendering a low SA value.

Out of interest, double and triple layer coatings were performed to evaluate effect of multi-layer coatings on the membranes' anti-wetting ability. As reported in Table 1, while SA showed no significant trend upon manipulation of coating layers, the CA decreased as coating layers increased. PP/6331-L2, though still having a satisfactory high CA hitting close to 150°, is yet to be ranked in the superhydrophobic category. CA of PP/6331-L3, however, dropped to $137.0 \pm 4.0^{\circ}$, akin to that of neat PP membrane. The result manifested that increasing the coating layer is unappealing, as PP agglomerates formed during the latter coating tend to fill in spaces in between PP clusters, reducing overall nano-scaled roughness while generating more micro-scaled spherulites (larger PP spherulites found in Figure 1(d)). As a result, less air is being trapped on the surface pockets and, again, water comes into a larger contact with the membrane surfaces, when compared relatively to membranes with fewer coated layers.

The changes of CA and SA are proportional to the membrane's surface roughness, where their interrelationship has been analyzed using AFM (Figure 2). Unsurprisingly, neat PP membrane reported the highest average roughness of 0.428 μm, compared to 0.321 and 0.418 μm for PP/6331-L1 and PP/6331-L3. As discussed earlier, the rough surface of neat PP membrane was attributed to the presence of crisscrossing micro-diameter fibers and the wide gap distance between fibers that formed the troughs, whereas for PP/6331-L1, the surface was layered by evenly distributed PP nano-clusters (Figure 1(b)), rendering the surface structure to appear saw-teeth-like. This structure has narrowed the gap distance between the valley's height and depth on the membrane surface, thus lowering the overall surface roughness (Figure 2(b)). The surface of PP/6331-L3, though also layered with PP coating, happened to be more hilly-like (Figure 1(d)), as PP agglomerates are lumping together on PP/6331-L3 rather than presenting as a discrete form as on PP/6331-L1. The bulging part of large spherulite showed peaks on the AFM graph (Figure 2(c)) while the grooves are mostly contributed by convex lining and gaps on the PP agglomeration network.

Despite the common understanding that higher roughness will increase CA and decrease SA values, the results in this study contrasted with the theory. A major discovery to be highlighted is that the high roughness has to be associated with peaks' evenness in order to maintain a superhydrophobic surface. As seen in Figure 2(a) and 2(c), overall, neat PP and PP/6331-L3 membranes comprise a higher ratio of micro-scaled peak-to-peak distance, with neat PP membrane having broader peaks. Also, their surface sectioning lines (2D graphs in Figure 2) run off irregularly from the center axis (dotted line), indicating the lack of surface homogeneity. In short, these two surfaces were unable

to contain sufficient air pockets to spike up the CAs. The water droplet, however, was unable to slide down from the surface of the neat PP membrane (Table 1, SA value more than 90°), due to the presence of deeper and wider grooves on the membrane surface. There is a high chance that water will impregnate into deep grooves of the neat PP membrane, making it the main reason for the membrane showing water-sticking behavior. In contrast, PP/6331-L3 contained micro-scaled PP spherulites as seen in Figure 1(d), which restrict direct interaction between water and membrane surface, hence allowing the water droplet to slide from the membrane surface with SA of $21.2 \pm 7.0°$. While performance of neat PP and PP/6331-L3 were not up to par, a single layer coating successfully rendered PP/6331-L1 superhydrophobic, transforming the Cassie-impregnating regime fully into the Cassie-Baxter state. In this case, the cohesive force within water droplets resting on the surface of PP/6331-L1 was greater than the water's adhesiveness towards the membrane surface. Hence, the water droplet remained intact in its spherical shape, and easily rolled off from the membrane surface. This finding was attributed to the narrow and consistent peak-to-peak distance (Figure 2(b)), as well as the evenness of the single layer coating.

Separation functionalities of the membranes were tested in DCMD with 35 g/L salt solution as feed and the results are tabulated in Figure 4. All membrane samples were able to reject over 99.99% of salt, but their flux differed across the performance test. Of all, neat PP membrane had the lowest flux at an average of 9.8 $kg/m^2 h$, followed by PP/6331-L3 at 11.0 $kg/m^2 h$. The average flux for PP/6331-L1 and PP/6331-L2, however, showed no distinct difference, with reported fluxes approximately 13.0 $kg/m^2 h$. As observed in SEM images in Figure 1, the surface pore sizes of the membrane were reduced after coating with layers of PP. Indeed, bigger pores should lead to higher flux, although only to a certain extent as further increment in pore radius to greater than 0.2 μm did not contribute much to a better flux, according to Li *et al.* (2014). Moreover, overly large pore size will extensively reduce liquid entry pressure of the membrane, which leads to a severe wetting issue (Sivakumar *et al.* 2014). Based on the SEM analysis (Figure 1), pore radius for all membranes in this work were greater than 0.2 μm, ranging from approximately 3 to 10 μm. This means the pore size reduction in coated membranes will not affect the DCMD flux.

The increment of fluxes for surface-coated membranes could be attributed to the improved CA and SA, as discussed earlier. When CA of a membrane was enhanced to a superhydrophobic state, its outstanding anti-wetting ability would be expected to 'lift up' the air–liquid interface to the top edge of the membrane (Yang *et al.* 2014). The dry areas between the air–liquid interface and valleys were responsible for water evaporation. The fluxes of PP/6331-L1 and PP/6331-L2 were thereby higher since they have larger effective evaporation area than neat PP and PP/6331-L3 membranes, as their CA suggested (Table 1). Furthermore, the water-sticking behavior observed in neat PP membrane would be detrimental to the flux. The strong adhesion behavior of water will potentially maintain a stagnant water layer on the membrane surface, which hindered effective mixing between bulk feed and feed solution adjacent to the membrane surface (Khalifa 2020). This in turn generated a larger

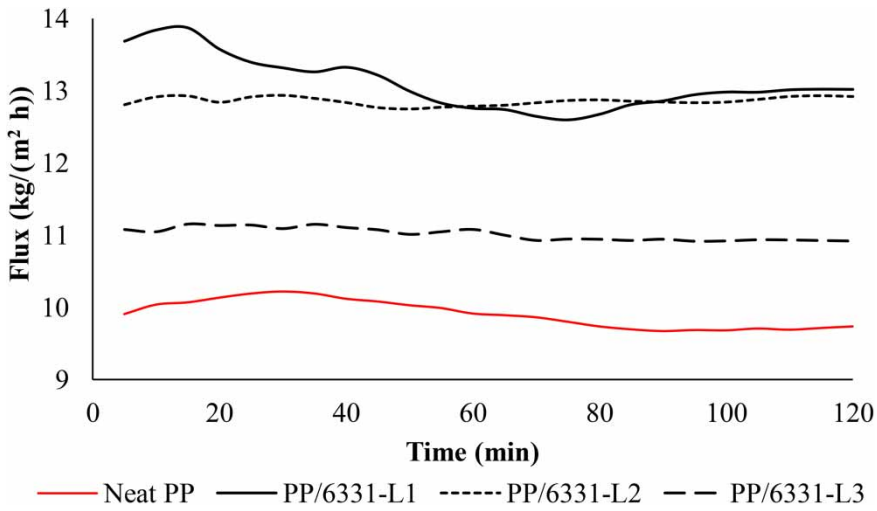


**Figure 4** | Flux of neat and surface modified membranes in 2 hr DCMD performance test.

temperature difference across the thermal boundary layer between bulk feed and the membrane surface. Following that, temperature polarization became more severe, which would translate into lower driving force of vapor across the membrane. Despite there being ways to maintain the driving force to counter the temperature polarization effect such as to increase feed temperature, this initiative is proven to be energy extensive and is not being encouraged (Shahu & Thombre 2019). The water adhering on the membrane surface would also facilitate membrane wetting (Teoh *et al.* 2020), subsequently reducing the effective evaporation area and, thus, lowering the permeate flux.

Due to the inversely proportional relationship between flux and thickness, the PP/6331-L3, which is the thickest membrane, has the lowest flux among its coated counterparts. This is because as membrane thickens, the distance between the liquid–vapor interface at which evaporation and condensation occur on both sides of the membrane becomes greater. Considering a longer vapor travelling path and the overlapping voids in the membrane, the vapor molecules have to undergo more collisions with the polymeric matrix before reaching the other side of the membrane. Hence, a higher mass transfer resistance was imposed on the vapor. In the case of this work, the impact of the adhered water layer on the membrane surface is more detrimental than the effect of increased membrane thickness, evidenced by the higher flux of PP/6331-L3 as compared to neat PP membrane, despite them having a similar CA (Table 1). While the membrane should be thin enough to minimize mass transfer resistance, there is a limitation whereby further decrease in membrane thickness induces greater conductive heat loss across the membrane. This heat loss will be translated into lower temperature gradient across the membrane, resulting in lower flux (Li *et al.* 2014). The neat PP and PP/6331-L1 may have suffered from this issue, as their flux dropped during the initial DCMD test, then stabilized after the counterbalance between the conductive and latent heat of vaporization. With all the analyses on hand, PP/6331-L1 with relatively higher flux, better anti-wetting performance (CA and SA) and surface roughness homogeneity was still deemed to be the best modified membrane.

PP/6331-L1 was then tested for its robustness and anti-wetting stability in a 60 hr long term DCMD separation process with operational parameters similar to those of the previous short term (2 hr) MD performance test (Figure 4). As observed in Figure 5, average flux of 13.2 kg/(m$^2$ h) was attained by PP/6331-L1 for the first 24 hr of the DCMD operation. This recorded flux coincides with the result obtained previously in the short term DCMD process, signifying the reproducibility of the modified electrospun PP membrane. At the 25th hr, the flux demonstrated a fall-off then remained stable until the 60th hr at an average flux of 12.0 kg/m$^2$ h, an 8.6% decline as compared to the first 24 hr flux.

Based on the long term DCMD result, it is reasonable to infer that there was negligible membrane pore wetting as salt rejection stabled at 99.99% throughout the separation performance test. The dwindling of flux at hour 25 is probably the consequence of concentration polarization.

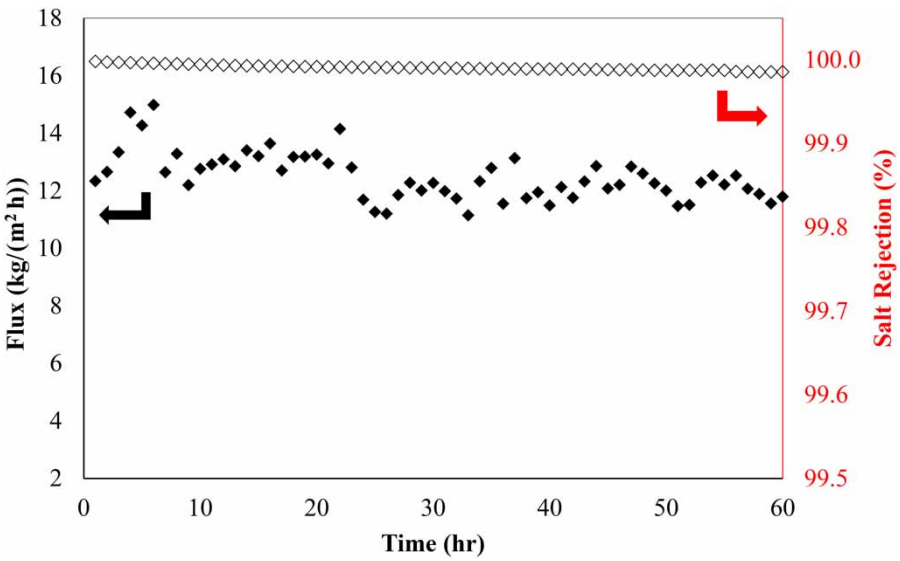


**Figure 5** | Flux and salt rejection of PP/6331-L1 in 60 hr long term DCMD performance test.

Though salt crystal in the flowing feed adjacent to the membrane surface is expected to have difficulties attaching to the membrane surface as PP/6331-L1 achieved superhydrophobic state, there are still chances that dissolved salt will deposit on the membrane surface. This is because cation $Na^+$ has the tendency to combine with surrounding water molecules but its diffusion through the membrane was hindered when water evaporated and transferred across the membrane pores in vapour form. The left-behind cations hence increase concentration and viscosity of salt solution at the boundary layer. Other than blocking membrane pores partially, the thickened concentration polarization layer will also result in lower flow rate at areas adjacent to the membrane surface, leading to decreased vapour pressure and hence lower permeate flux (Shao *et al.* 2019).

The performance of the modified membrane in this work is compared with other literature. As summarized in Table 2, salt rejection and the flux of modified membrane in the present study are comparable to other membranes listed, be they laboratory cast or commercially available. Also, it is obvious that most of the researches favor vacuum membrane distillation operation over DCMD (present work) when PP was used as the base membrane material. Hollow fiber PP membranes are also used in many MD desalting related studies. It also came to our attention that research works relating to MD employing PP membranes are scanty, not to mention there is currently no available study deploying an electrospun PP membrane in the MD desalination process, as far as we know. This is probably due to the detrimental water pinning effect exhibited by PP electrospun membranes, despite having high CA in nature. In fact, SA, which is one of the determining factors towards excellent MD performance, is not examined in other researches listed in Table 2. Wrapping up, embracing a facile solvent-exchange surface coating technique, this work successfully addresses the parahydrophobic issue faced by a neat electrospun PP membrane without compromising its porosity. Moreover, the MD operating duration of the current work is much longer than those reported in other literatures, further strengthening the stability of its anti-wetting property in a long-hour MD process.

**Table 2** | Comparison of flux and salt rejection of membranes treating 35 g/L NaCl aqueous solution employing MD reported in literature

| Membranes | $\varepsilon$ | CA/SA | DCMD conditions | Flux (kg/m$^2$ h) | SR (%) | Reference |
|---|---|---|---|---|---|---|
| [a]Perfluorinated silane modified PP hollow fiber membrane | 0.41 | CA: 157°<br>SA: – | $T_f$: 80 °C<br>$P_v$: 100 kPa<br>F: –<br>D: – | ~0.9 | 99.8 | Xu *et al.* (2017) |
| [a]Fluorination and silification of PDA/PEI coated commercial PP hollow fiber membrane | – | CA: >150°<br>SA: – | $T_f$: 70 °C<br>$P_v$: 95 kPa<br>F: –<br>D: 46 hr | ~12.0 | >99.9 | Zhong *et al.* (2017) |
| [a]Fluorinated functionalized $SiO_2$ deposited PP flat sheet microporous membrane | – | CA: 159°<br>SA: – | $T_f$: 80 °C<br>F: 0.09 L/min<br>$P_v$: 96 kPa<br>D: 50 hr | ~11.0 | 99.99 | Wang *et al.* (2019) |
| [b]Commercial PVDF membrane | 0.57 | CA: 119.7°<br>SA: – | ΔT: 40 °C<br>F: 0.6 L/min<br>D: 50 hr | 21.0 | 99.99 | Deng *et al.* (2019) |
| [b]Commercial PTFE membrane | 0.75 | CA: 124.6°<br>SA: – | ΔT: 60 °C<br>F: 0.36 L/min<br>D: 6 hr | 10.2 | 99.95 | Sadeghzadeh *et al.* (2020) |
| [b]Solvent-exchange PP coating on commercial PP electrospun membrane | 0.76 | CA: 152.2°<br>SA: 12.5° | ΔT: 40 °C<br>F: 0.3 L/min<br>D: 60 hr | 13.0 | 99.99 | This work |

[a]Vacuum membrane distillation.
[b]Direct contact membrane distillation.
Abbreviations: SR, salt rejection; $T_f$, feed temperature; $P_v$, vacuum pressure; F, flow rate; D, MD operation duration; ΔT, temperature difference between feed and permeate; PDA, polydopamine; PEI, polyethyleneimine; PTFE, polytetrafluoroethylene.

## CONCLUSIONS

Layering PP polymer onto electrospun membrane by solvent-exchange has proven to improve the membrane's hydrophobicity and surface homogeneity, subsequently resolving the issue of strong water adhesion on electrospun membranes. These improvements, along with the non-affected porosity of the membrane after PP coating, are predominant for MD flux enhancement. In this study, the single layer coated membrane, PP/6331-L1, which successfully achieved the superhydrophobic state was reported to have the best anti-wetting and flux performances. With recorded average CA of 152° and SA of 12.5°, PP/6331-L1 was able to improve DCMD flux by 30% as compared to the neat membrane when its separation performance was examined under 2 hr DCMD operation. Furthermore, PP/6331-L1 demonstrated superior capability to resist membrane pore wetting in a 60 hr long term DCMD desalination process by maintaining stable permeate flux and salt rejection of 99.9%. In this work, it was also found that, despite a rough surface being preferable for a better DCMD separation, the surface roughness has to be even with tiny spherulites, to signify the membrane's superhydrophobic character. To our best knowledge, this study is a pioneer in using a PP electrospun superhydrophobic modified membrane to treat high salinity water employing DCMD. When compared to other DCMD operations, separation performance of PP/6331-L1 was found to be competitive. Also, attributed to the simplicity of the modification process to achieve outstanding results, the superhydrophobic membrane modified via polymer coating hence has potential for aquaculture wastewater treatment application.

## ACKNOWLEDGEMENT

This work was supported by MOHE Transdisciplinary Research Grant Scheme (TRGS/1/2018/USM/01/5/1; Account No. TRGS/203/PJKIMIA/67612001). Chin Jing Yi acknowledges academic financial support awarded by Universiti Sains Malaysia Fellowship Scheme.

## DATA AVAILABILITY STATEMENT

All relevant data are included in the paper or its Supplementary Information.

## REFERENCES

Andrews, H. G., Eccles, E. A., Schofield, W. C. E. & Badyal, J. P. S. 2011 Three-dimensional hierarchical structures for fog harvesting. *Langmuir* **27** (7), 3798–3802. https://doi.org/10.1021/la2000014.

Ariga, K., Ahn, E., Park, M. & Kim, B.-S. 2019 Layer-by-layer assembly: recent progress from layered assemblies to layered nanoarchitectonics. *Chemistry – An Asian Journal* **14** (15), 2553–2566. https://doi.org/10.1002/asia.201900627.

Boubakri, A., Hafiane, A. & Al Tahar Bouguecha, S. 2015 Nitrate removal from aqueous solution by direct contact membrane distillation using two different commercial membranes. *Desalination and Water Treatment* **56** (10), 2723–2730. https://doi.org/10.1080/19443994.2014.981408.

Deng, L., Li, P., Liu, K., Wang, X. & Hsiao, B. S. 2019 Robust superhydrophobic dual layer nanofibrous composite membranes with a hierarchically structured amorphous polypropylene skin for membrane distillation. *Journal of Materials Chemistry A* **7** (18), 11282–11297. https://doi.org/10.1039/C9TA02662B.

Erbil, H. Y., Demirel, A. L., Avcı, Y. & Mert, O. 2003 Transformation of a simple plastic into a superhydrophobic surface. *Science* **299** (5611), 1377. https://doi.org/10.1126/science.1078365.

Feng, Y., Zhang, Y., Xi, J., Zhu, Y., Wang, N., Xia, F. & Jiang, L. 2008 Petal effect: a superhydrophobic state with high adhesive force. *Langmuir* **24**, 4114–4119. https://doi.org/10.1021/la703821 h.

Franco, J. A., Kentish, S. E., Perera, J. M. & Stevens, G. W. 2008 Fabrication of a superhydrophobic polypropylene membrane by deposition of a porous crystalline polypropylene coating. *Journal of Membrane Science* **318** (1), 107–113. https://doi.org/10.1016/j.memsci.2008.02.032.

Khalifa, A. E. 2020 Flux enhanced water gap membrane distillation process-circulation of gap water. *Separation and Purification Technology* **231**, 115938. https://doi.org/10.1016/j.seppur.2019.115938.

Koschikowski, J., Wieghaus, M. & Rommel, M. 2003 Solar thermal driven desalination plants based on membrane distillation. *Water Supply* **3** (5–6), 49–55. https://doi.org/10.2166/ws.2003.0149.

Krajenta, J., Pawlak, A. & Galeski, A. 2016 Deformation of disentangled polypropylene crystalline grains into nanofibers. *Journal of Polymer Science Part B: Polymer Physics* **54** (19), 1983–1994. https://doi.org/10.1002/polb.24105.

Krajenta, J., Safandowska, M. & Pawlak, A. 2019 The re-entangling of macromolecules in polypropylene. *Polymer* **175**, 215–226. https://doi.org/10.1016/j.polymer.2019.05.015.

Lai, Y., Gao, X., Zhuang, H., Huang, J., Lin, C. & Jiang, L. 2009 Designing superhydrophobic porous nanostructures with tunable water adhesion. *Advanced Materials* **21** (37), 3799–3803. https://doi.org/10.1002/adma.200900686.

Li, Z., Peng, Y., Dong, Y., Fan, H., Chen, P., Qiu, L. & Jiang, Q. 2014 Effects of thermal efficiency in DCMD and the

preparation of membranes with low thermal conductivity. *Applied Surface Science* **317**, 338–349. https://doi.org/10.1016/j.apsusc.2014.07.080.

Li, X., García-Payo, M. C., Khayet, M., Wang, M. & Wang, X. 2017 Superhydrophobic polysulfone/polydimethylsiloxane electrospun nanofibrous membranes for water desalination by direct contact membrane distillation. *Journal of Membrane Science* **542**, 308–319. https://doi.org/10.1016/j.memsci.2017.08.011.

Liao, Y., Wang, R. & Fane, A. G. 2013 Engineering superhydrophobic surface on poly(vinylidene fluoride) nanofiber membranes for direct contact membrane distillation. *Journal of Membrane Science* **440**, 77–87. https://doi.org/10.1016/j.memsci.2013.04.006.

Liu, Y., Lv, J., Feng, J., Liu, Q., Nan, F. & Xie, S. 2019 Treatment of real aquaculture wastewater from a fishery utilizing phytoremediation with microalgae. *Journal of Chemical Technology and Biotechnology* **94** (3), 900–910. https://doi.org/10.1002/jctb.5837.

Lu, X., Zhang, C. & Han, Y. 2004 Low-density polyethylene superhydrophobic surface by control of its crystallization behavior. *Macromolecular Rapid Communications* **25**, 1606–1610. https://doi.org/10.1002/marc.200400256.

Qu, D., Sun, D., Wang, H. & Yun, Y. 2013 Experimental study of ammonia removal from water by modified direct contact membrane distillation. *Desalination* **326**, 135–140. https://doi.org/10.1016/j.desal.2013.07.021.

Sadeghzadeh, A., Bazgir, S. & Shirazi, M. M. A. 2020 Fabrication and characterization of a novel hydrophobic polystyrene membrane using electroblowing technique for desalination by direct contact membrane distillation. *Separation and Purification Technology* **239**, 116498. https://doi.org/10.1016/j.seppur.2019.116498.

Sawyer, L., Grubb, D. & Meyers, G. F. 2008 *Polymer Microscopy*. Springer-Verlag, New York, USA.

Seyed Shahabadi, S. M., Rabiee, H., Seyedi, S. M., Mokhtare, A. & Brant, J. A. 2017 Superhydrophobic dual layer functionalized titanium dioxide/polyvinylidene fluoride-co-hexafluoropropylene ($TiO_2$/PH) nanofibrous membrane for high flux membrane distillation. *Journal of Membrane Science* **537**, 140–150. https://doi.org/10.1016/j.memsci.2017.05.039.

Shahu, V. T. & Thombre, S. B. 2019 Analysis and optimization of a new cylindrical air gap membrane distillation system. *Water Supply* **20** (1), 361–371. https://doi.org/10.2166/ws.2019.164.

Shao, Y., Han, M., Wang, Y., Li, G., Xiao, W., Li, X., Wu, X., Ruan, X., Yan, X., He, G. & Jiang, X. 2019 Superhydrophobic polypropylene membrane with fabricated antifouling interface for vacuum membrane distillation treating high concentration sodium/magnesium saline water. *Journal of Membrane Science* **579**, 240–252. https://doi.org/10.1016/j.memsci.2019.03.007.

Sivakumar, M., Ramezanianpour, M. & O'halloran, G. 2014 Brackish water treatment for reuse using vacuum membrane distillation process. *Water Supply* **15** (2), 362–369. https://doi.org/10.2166/ws.2014.116.

Teoh, G. H., Chin, J. Y., Ooi, B. S., Jawad, Z. A., Leow, H. T. L. & Low, S. C. 2020 Superhydrophobic membrane with hierarchically 3D-microtexture to treat saline water by deploying membrane distillation. *Journal of Water Process Engineering* **37**, 101528. https://doi.org/10.1016/j.jwpe.2020.101528.

Van der Meer, D. W. 2003 *Structure-Property Relationships in Isotactic Polypropylene: the Influence of Chain Architecture and Nucleation on Crystallization, Morphology and Mechanical Properties*. PhD Thesis, Dutch Polymer Institute, University of Twente, Netherlands.

Wang, P. & Chung, T.-S. 2015 Recent advances in membrane distillation processes: membrane development, configuration design and application exploring. *Journal of Membrane Science* **474**, 39–56. https://doi.org/10.1016/j.memsci.2014.09.016.

Wang, X., Liu, R., Wu, M., Wang, Z. & Huang, Y. 2009 Effect of chain disentanglement on melt crystallization behavior of isotactic polypropylene. *Polymer* **50**, 5824–5827. https://doi.org/10.1016/j.polymer.2009.10.002.

Wang, Y., He, G., Shao, Y., Zhang, D., Ruan, X., Xiao, W., Li, X., Wu, X. & Jiang, X. 2019 Enhanced performance of superhydrophobic polypropylene membrane with modified antifouling surface for high salinity water treatment. *Separation and Purification Technology* **214**, 11–20. https://doi.org/10.1016/j.seppur.2018.02.011.

Xu, Z., Liu, Z., Song, P. & Xiao, C. 2017 Fabrication of superhydrophobic polypropylene hollow fiber membrane and its application in membrane distillation. *Desalination* **414**, 10–17. https://doi.org/10.1016/j.desal.2017.03.029.

Yang, C., Li, X.-M., Gilron, J., Kong, D.-f., Yin, Y., Oren, Y., Linder, C. & He, T. 2014 CF4 plasma-modified superhydrophobic PVDF membranes for direct contact membrane distillation. *Journal of Membrane Science* **456**, 155–161. https://doi.org/10.1016/j.memsci.2014.01.013.

Zhong, W., Hou, J., Yang, H.-C. & Chen, V. 2017 Superhydrophobic membranes via facile bio-inspired mineralization for vacuum membrane distillation. *Journal of Membrane Science* **540**, 98–107. https://doi.org/10.1016/j.memsci.2017.06.033.

First received 8 July 2020; accepted in revised form 23 October 2020. Available online 5 November 2020